Acta Mechanica Solida Sinica, Vol. 34, No. 6, December, 2021, 937–953 ISSN 1860-2134
https://doi.org/10.1007/s10338-021-00285-1

Experiment and Numerical Simulation on the Dynamic Response of Foam-Filled Tubes Under Lateral Blast Loading

Zhifang Liu[1,2] **Tianhui Zhang**[1,2] **Shiqiang Li**[1,2] **Jianyin Lei**[1,2] **Zhihua Wang**[1,2⋆]

([1] *Institute of Applied Mechanics, College of Mechanical and Vehicle Engineering, Taiyuan University of Technology, Taiyuan 030024, China*)

([2] *Shanxi Key Laboratory of Material Strength and Structural Impact, Taiyuan University of Technology, Taiyuan 030024, China*)

Received 30 April 2021; revision received 28 September 2021; Accepted 29 September 2021;
published online 11 December 2021

ABSTRACT The dynamic response and energy absorption performance of foam-filled tubes under lateral external blast loading were investigated experimentally and numerically. A series of blast tests for the foam-filled tubes with different geometric parameters were carried out by the use of the ballistic pendulum system. Experimental results were compared with the numerical simulation results employing the software ABAQUS. The results showed that the finite element (FE) analysis was in good agreement with the experimental data. The effects of the diameter and wall thickness of the outer tube, the TNT explosive charge mass, and the standoff distance on the deformation modes, the blast resistance, and the energy absorption performance of the foam-filled tubes were investigated. Three deformation modes of the foam-filled tubes were observed under the lateral external blast loading, including local plastic deformation, large plastic deformation with an elliptic shape, and the tearing of the outer tube. The result revealed that the introduction of the foam core played a vital role in the deflection and energy absorption capacity of the structure. This study provided effective guidelines for designing foam-filled tubes with high energy absorption efficiency.

KEY WORDS Foam-filled tubes, Aluminum foam, Lateral blast loading, Numerical simulation

1. Introduction

The optimal design of structural crashworthiness is a hot topic that has been widely concerned by engineers and researchers. It is a very practical problem to make the structure have better energy absorption with the same mass or have lighter weight under the same crashworthiness condition. The thin-walled metal tubes are commonly used as energy-absorbing materials in the field of industrial applications. With the increasing security requests and frequent occurrence of accidental or intentional explosions, a deep understanding of the dynamic response of thin-walled and filled tubes under impact or blast loading is of great importance. Therefore, the mechanical behavior of the thin-walled structure, the aluminum foam sandwiched structure, and the filling structure in protective engineering have been investigated widely [1–3].

⋆ Corresponding author. E-mail:wangzh077@163.com

Compared with traditional materials, metal foam material has the characteristics of lightweight, high specific strength, high specific stiffness, and excellent energy absorption capacity. Hall et al. [4] firstly studied the energy absorption performance of aluminum, brass, and titanium foam-filled tubes under transverse impact loading, and the aluminum foam-filled tubes showed the best energy absorption characteristics. Fan et al. [5] studied the mechanical response of short empty and sandwiched circular tubes under the dynamic lateral load. The results showed that the plastic energy dissipation of the tubes under the dynamic impact load was mainly realized by the movement of the plastic hinge along the circular direction.

Furthermore, Fan et al. [5] and Shen et al. [6] conducted experimental studies on the transverse crushing of thin-walled sandwiched circular tube structures filled with aluminum foam. Three different crushing patterns were identified, and the progressive collapse process and the load–displacement curve were obtained. The progressive collapse process of the foam-filled tubes was simulated numerically and compared with the experimental data, showing good agreement. The energy absorption capacity of the foam-filled sandwiched tube was larger than the sum of that of the individual inner tube, outer tube, and foam core layer.

Besides the sandwiched circular tube, other sections in the shape of a sandwiched structure under lateral loading also attracted the attention of researchers including multi-cell thin-walled triangular empty tubes [7], internally nested circular tubes [8], and sandwiched tubes with the agglomerated cork core [9]. Liu et al. [10] also investigated the lateral crushing responses of aluminum honeycombs filled with the expanded polypropylene (EPP) foam. The result showed that all the foam-filled panels showed larger energy absorption than the sum of that of bare honeycomb and the EPP foam separately under lateral crushing.

Under blast loading, the introduction of the foam core plays a vital role in the deformation modes and shock resistance of the whole specimen. To achieve the minimum specific deflection of the outer face sheet and the maximum specific energy absorption, numerous studies on thin-walled structures and aluminum foam sandwiched and filled structures have been conducted in the past decade [11–13]. Liu et al. [14] investigated the dynamic responses and explosive resistance of all-metallic sandwich-walled hollow cylinders with graded aluminum foam cores under identical air blast loading using the FE simulations. It was found that the radial deflection of graded cylinders was smaller than that of conventional ungraded ones, and their blast resistance was superior to that of conventional ungraded ones. Jing et al. [15, 16] investigated the dynamic response of cylindrical sandwiched shells with metallic foam cores under blast loading by experiments, numerical simulations (LS-DYNA), and theoretical analysis. The loading intensity and geometric configuration had significant effects on the deformation/failure, deflection response, and energy absorption of sandwiched shells. With an increase in the impulse level and the core relative density, the energy absorption capability of cylindrical sandwiched shells monotonically increased and decreased, respectively. Liang et al. [17] used the response surface method and the non-dominated sorting genetic algorithm to determine the optimal face-sheet thickness and core gradient. However, with the improvement in the utilization of the aluminum foam-filling tubes, their shock resistance and energy absorption capability under blast loading need to be further studied.

For circular tubes, Wierzbicki and Fatt [18] used the string-on-foundation model to study the large-amplitude transient response of plastic cylindrical shells, derived simple formulas for the ballistic limit of an unstiffened shell under the missile impact, and determined the critical impulse to rupture the stiffened shell. Song et al. [19] presented an analytical model to analyze the plastic deformation of steel circular tubes and obtained the deflection and deformation angle of the tubes. Yuen et al. [20] presented a series of experimental and numerical analyses on cylindrical shells under the lateral blast load. The results were compared with the analytical solution developed by Wierzbicki and Fatt [19], and the numerical simulations showed good correlations.

In this paper, the dynamic response of aluminum foam-filled tubes was investigated experimentally and numerically. The experimental processes and results of foam-filled tubes under lateral blast loading are described and shown in Sect. 2. Then, the impulse of foam-filled tubes under lateral blast loading is analyzed theoretically in Sect. 3. The numerical simulation results of the foam-filled tubes are presented and discussed in Sect. 4. The experimental and numerical results on the final deflections and deformation modes of the specimens showed good agreement. Besides the deformation peculiarities

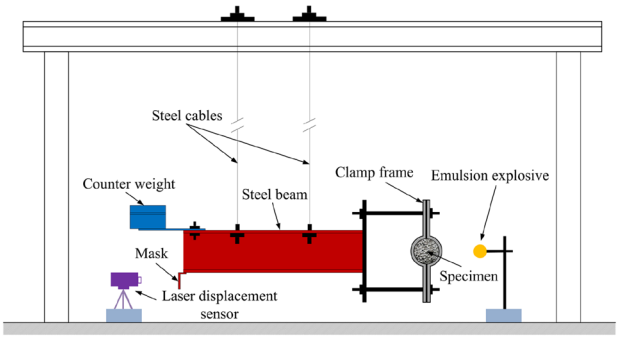

Fig. 1. The basic frame of the blast experiment

and the blast resistance, the deformation process, the permanent non-dimensional deflection, and the contribution ratio of energy absorption by each part are also discussed in Sect. 5.

2. Experimental Investigations

2.1. Materials and Procedure

A typical configuration of the foam-filled tube was composed of two parts: an outer cylindrical tube and a core made of closed-cell aluminum foams. The average relative density of the aluminum foams was 15%. The outer tube had different diameters D (76 mm, 89 mm, and 101 mm), wall thicknesses h (0.7, 0.8, and 0.9 mm), and a uniform span L (380 mm). The basic frame of the blast experiment is shown in Fig. 1. The tube was peripherally clamped between four semicircular steel frames. Four semicircular fixtures with a width of 50 mm and φ18 mm bolts were used to clamp the tube specimens. For the test specimens with the outer tube diameter of D =76 and 89 mm, a semicircular spacer with a thickness of 25 and 12 mm should be added, respectively.

A four-cable ballistic pendulum system was employed to measure the impulse imparted on the specimens as shown in Fig. 2. The foam-filled tubes were mounted to the pendulum. Thus, the impulse imparted to the tubes could be determined from the pendulum's swing. Based on the time-history curve of the deflection recorded by a laser displacement transducer, the impulse on the tube specimens could be further obtained [13].

2.2. Experimental Results

The experimental results are divided into two parts: (1) the quantitative results including the impulse acting on the foam-filled tubes and the final permanent deflection; (2) the typical deformation modes of the foam-filled tubes under lateral blast loading. Details of these results are presented in Sects. 2.2.1 and 2.2.2, respectively.

2.2.1. Quantitative Results of the Impulse and the Deflection

The impulse of the foam-filled tube under blast loading was calculated using the time-history curve of the deflection obtained by a laser displacement transducer (Fig. 3). In the blast test, the motion of the ballistic pendulum could be simplified to be described by Eq. [21]:

$$M\frac{\mathrm{d}^2x}{\mathrm{d}^2t} + C_0\frac{\mathrm{d}x}{\mathrm{d}t} + \frac{Mg}{R_0}x = 0 \tag{1}$$

where M, x, and R_0 are the total mass, horizontal displacement, and motion radius of the pendulum, respectively, and C_0 is a damping coefficient. The solution of Eq. (1) can be expressed as:

$$x = \frac{x_0}{\omega}\mathrm{e}^{-\eta t}\sin\omega t \tag{2}$$

where $\omega = \sqrt{g/R_0 - \eta^2}$, $\eta = \frac{C_0}{2M}$, and x_0 is the initial displacement of the ballistic pendulum. The vibration period of the ballistic pendulum is $T = 2\pi/\omega$. Defining x_1 and x_2 as the deflections at $t_1 = T/4$ and $t_2 = 3T/4$, respectively, and substituting them into Eq. (2), we can obtain the following

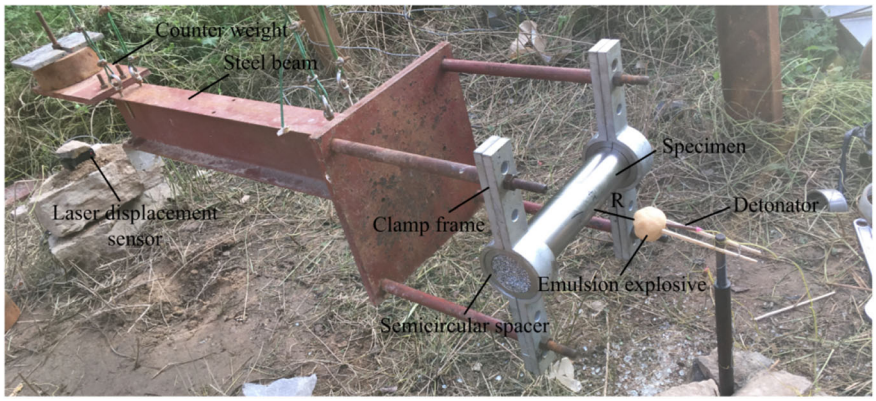

Fig. 2. Experimental setup of the ballistic pendulum system

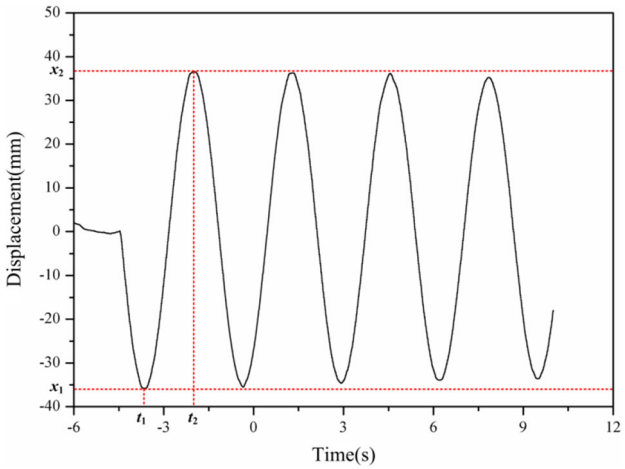

Fig. 3. Time-history curve of the displacement of the pendulum (Test No. 1)

formulas:

$$x_1 = \frac{T}{2\pi} \mathrm{e}^{-\frac{\eta T}{4}} x_0 \tag{3}$$

$$x_2 = \frac{T}{2\pi} \mathrm{e}^{-\frac{3\eta T}{4}} x_0 \tag{4}$$

Then, η can be expressed as:

$$\eta = 2 \ln \frac{x_1}{x_2} / T \tag{5}$$

By substituting the solution of η into Eq. (3), the initial displacement of the ballistic pendulum x_0 can be obtained as:

$$x_0 = \frac{2\pi}{T} \mathrm{e}^{\frac{\eta T}{4}} x_1 \tag{6}$$

Therefore, the impulse acting on the tube is given as:

$$I_E = M x_1 \frac{2\pi}{T} \mathrm{e}^{\frac{\eta T}{4}} \tag{7}$$

For the present tests, the motion radius of the pendulum R_0 was 2.95 m. The maximum rotation angle was approximately 2.6°, which was less than 5° and acceptable.

Table 1. **Specifications of the foam-filled tubes and experimental results**

Test no.	M(kg)	ρ^* (%)	D(mm)	h(mm)	W_s (g)	R(mm)	I_E (N· s)	w(mm)
1	96.8	16.1	76	0.7	30	40	7.1	14
2	96.7	15.6	76	0.7	50	40	12.9	22.1
3	96.7	14.8	76	0.7	80	40	17.7	–
4	95.9	16.1	89	0.8	50	40	12.4	23.5
5	95.2	17	101	0.7	50	40	13.7	24.4
6	96.8	15.4	76	0.8	50	40	10.4	18.8
7	96.9	16.8	76	0.9	50	40	12	19.7
8	96.8	15.7	76	0.7	100	60	–	12
9	96.8	13.9	76	0.7	100	80	–	11
10	96.8	13.7	76	0.7	100	40	21.2	54.6

According to the data recorded and measured after the test, the blast impulse of the specimen and the final permanent deflection at the central point (w) were examined. Table 1 lists the experimental material parameters, the impulse, and the final midpoint deflection values under different load conditions. It should be noted that a part of the blast impulse acting on the steel frame clamping the specimen reduced the actual impulse acting on the specimen compared with the total impact measured by the ballistic pendulum. Due to the effects of the experimental environment, the time-history curves of the displacement for Test No. 8 and No. 9 were not obtained by a laser displacement sensor. The impulse of the two specimens could not be calculated according to Eq. (7).

Figure 4 presents the experimental results of the aluminum foam-filled tubes under lateral blast loading. In the course of the experiment, it was impossible to ensure that the explosive initiation point of blast loading was at the center of the foam-filled tube. The shape of the explosive was approximately spherical, leading to a certain error in the experimental results. The typical deformation modes of the foam-filled tubes under lateral blast loading will be discussed in detail in Sect. 2.2.2.

2.2.2. Deformation Modes

The deformation modes of the foam-filled tubes under lateral blast loading could be divided into local plastic deformation, large plastic deformation with an elliptical shape, and the tearing of the outer tube (Fig. 5), which were similar to the cylindrical tubes proposed by Yuen et al. [20] It could be seen that the explosive charge mass, the wall thickness of the outer tube, and the standoff distance played indispensable roles in the dynamic response of the foam-filled tubes (Fig. 4). Furthermore, the deformation area of the foam-filled tubes increased with an increase in the explosive charge mass. As the wall thickness and the standoff distance of the test specimen increased, the deformation range decreased. In the whole experiment, only Test No. 3 (W_s = 80 g, h = 0.7 mm, and R = 40 mm) showed a deformation mode of tearing of the outer tube.

To observe the deformation mode of the foam core, the specimen was treated by the wire cutting technique. The typical failure modes of the foam-filled tubes with different explosive charge masses, wall thicknesses, and standoff distances are shown in Figs. 6, 7, and 8, respectively. It was obvious that an increase in the explosive charge mass improved the impulse and the midpoint deflection of the foam-filled tubes. Also, an excessive explosive charge mass caused tearing of the outer tube. The wall thickness had little effect on the impulse and the midpoint deflection of the foam-filled tubes. As the standoff distance increased, the impulse and the midpoint deflection decreased. Because of the increased standoff distance, the blast load did not act on the center of the foam-filled tubes. Furthermore, the density of the foam core was uneven, which made the deformation modes in Test No. 8 and No. 9 inconsistent with the typical deformation mode.

From the axial sections and cross-sections, it could be seen that all the foam cores were characterized by crushed and uncompressed regions. The crushing of the foam core was accompanied by the generation of a crater in the central zone. In general, the foam core was progressively compressed and then fully compacted by the densification strain. It was observed that with an increase in the explosive charge mass, the range of the core compression increased. The tearing of the outer tube did not affect the deformation mode of the foam core, and the variation in the wall thicknesses had no significant

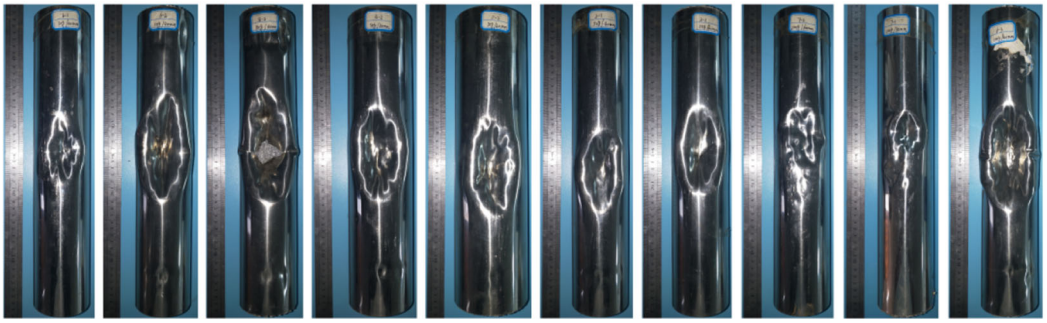

Test No.	1	2	3	4	5	6	7	8	9	10
W_s(g)	30	50	80	50	50	50	50	100	100	100
h(mm)	0.7	0.7	0.7	0.8	0.7	0.8	0.9	0.7	0.7	0.7
R(mm)	40	40	40	40	40	40	40	60	80	40
D(mm)	76	76	76	89	101	76	76	76	76	76

Fig. 4. Experimental results of the aluminum foam-filled tubes under lateral blast loading

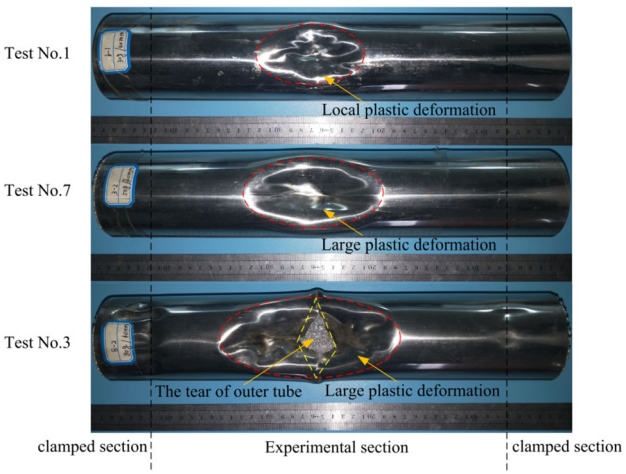

Fig. 5. Typical deformation modes of the aluminum foam-filled tubes under lateral blast loading

effect on the compression range of the core layer. As the standoff distance increased, the range of the core compression decreased. The foam core in Test No. 10 and No. 3 deformed significantly due to the large blast impulse. For other foam-filled tubes, there were craters with compaction on the blasting surface.

During the experiment, only the impulse acting on the system and the final deformation of the foam-filled tubes were obtained. The deformation mechanism of the foam-filled tubes under lateral blast loading and the duration of blast loading should be further analyzed by numerical simulations.

3. Calculation of the Theoretical Impulse

For spherical explosives, Henrych [22] presented a series of relevant empirical formulas. The specific impulse can be calculated as follows:

$$i_r = A^* \frac{\sqrt[3]{W^2}}{R} (\mathrm{kg \cdot s \cdot m^{-2}}), \quad R \leq 0.5\sqrt[3]{W}(\mathrm{m}) \tag{8}$$

$$i_r = 24\frac{W}{R^2} (\mathrm{kg \cdot s \cdot m^{-2}}), \quad R < 0.25\sqrt[3]{W}(\mathrm{m}) \tag{9}$$

$$W = W_s Q_{Ws}/Q_{WT} \tag{10}$$

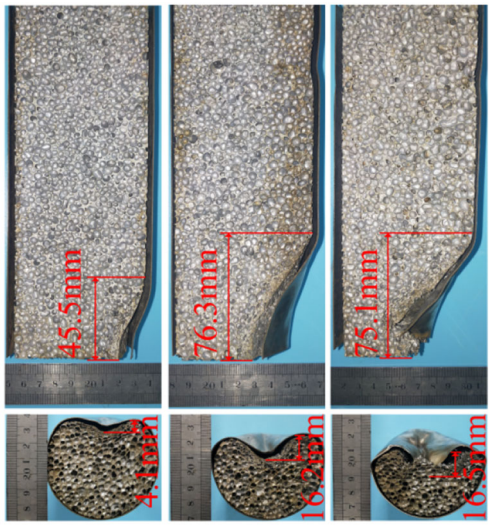

Test No.	1	2	3
W_s(g)	30	50	80
h(mm)	0.7	0.7	0.7
R(mm)	40	40	40
D(mm)	76	76	76
I_E(N·s)	7.1	12.9	17.7
w(mm)	14	22.1	Tearing

Fig. 6. Photographs showing the typical failure of foam-filled tubes with different explosive charge masses

where $A^* = 50 - 60$, R is the standoff distance, W is the TNT charge mass, W_s is the actual mass of the explosive, and Q_{Ws} and Q_{WT} are the explosion heat ratio of the actual explosive and TNT, respectively. It was the emulsified explosives that we used in this study and $Q_{Ws}/Q_{WT} = 0.7$.

The blast pressure distribution in the foam-filled tubes is a very complicated problem related to the geometry of the explosive, the charge distance, and the property of the fluid in the surrounding environment. Based on the research on cylindrical tubes under blast loading [23], a pressure distribution model for a foam-filled structure was designed as shown in Fig. 9. The approximate equation of the impulse can be expressed as follows:

$$P(x,\theta,t) = P_0 \mathrm{e}^{-\frac{t}{\tau}} f(x) g(\theta) \tag{11}$$

where P_0 is the peak pressure applied on the structure, and $f(x)$ and $g(\theta)$ are the initial pressure distribution functions in the axial and the circumferential directions, respectively. The characteristic time constant was $\tau = 25\mu s$, $f(x) = \cos^2(\pi x/L)$, and $g(\theta) = \sin\theta$ [23]. Therefore, the approximate equation of the foam-filled tubes under blast loading is expressed as follows:

$$P(x,\theta,t) = P_0 \mathrm{e}^{-\frac{t}{\tau}} \cos^2(\pi x/L) \sin(\theta) \tag{12}$$

The total impulse applies to the structure is calculated as follows:

$$I_T = 4\int_0^{L/2}\int_0^{\pi/2}\int_0^{\infty} p(x,\theta,t)\frac{D}{2}\mathrm{d}x\mathrm{d}\theta\mathrm{d}t = \frac{1}{2}P_0 DL\tau \tag{13}$$

In the blast experiment, all the foam-filled tubes satisfied the condition of Eq. (9). Assuming that the theoretical impulse $I_T = i_r DL$ and by plugging it into Eq. (13), the theoretical peak pressure P_0 can be derived as follows:

$$P_0 = 2I_T/DL\tau = 2i_r/\tau \tag{14}$$

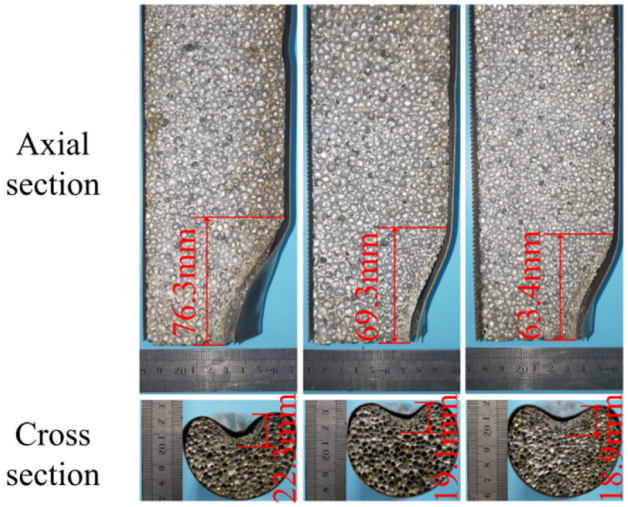

Test No.	2	6	7
W_s(g)	50	50	80
h(mm)	0.7	0.8	0.9
R(mm)	40	40	40
D(mm)	76	76	76
I_E(N·s)	12.9	10.4	12
w(mm)	22.1	18.8	19.7

Fig. 7. Photographs showing the typical failure of foam-filled tubes with different wall thicknesses

Table 2. **Comparison of the experimental and theoretical impulse**

Test No.	W (g)	D (mm)	R (mm)	P_0 (MPa)	i_r (kg· s· m^{-2})	I_E (N· s)	I_T (N· s)	Error $(I_T - I_E)/I_E \times 100\%$
1	21	76	40	25.2	315	7.1	6.7	−5.6%
2	35	76	40	42.1	525	12.9	12.2	−5.4%
3	56	76	40	67.3	840	17.7	17.9	1.1%
4	35	89	40	42.1	525	12.4	13.1	5.6%
5	35	101	40	42.1	525	13.7	14.9	8.8%
6	35	76	40	42.1	525	10.4	11.2	7.7%
7	35	76	40	42.1	525	12	11.2	−6.7%
8	70	76	60	37.2	466.7	–	9.9	–
9	70	76	80	21.1	262.5	–	5.6	–
10	70	76	40	83.8	1050	21.2	22.3	5.2%

Table 2 lists the theoretical impulse compared with the experimental results, where good agreement can be observed. On the other hand, with an increase in the initiation distance, it could not be guaranteed that the position of the explosive load acting on the foam-filling tube was at the center of the specimen as shown in Fig. 4.

Equations (8) and (9) are the empirical formulas for the impulse of a spherical explosive acting on an obstacle, and there was good agreement between the current experimental results and the theoretical predictions. Therefore, Eqs. (8) and (9) can be used to estimate the accidental air blast impulse under the current experimental charge condition.

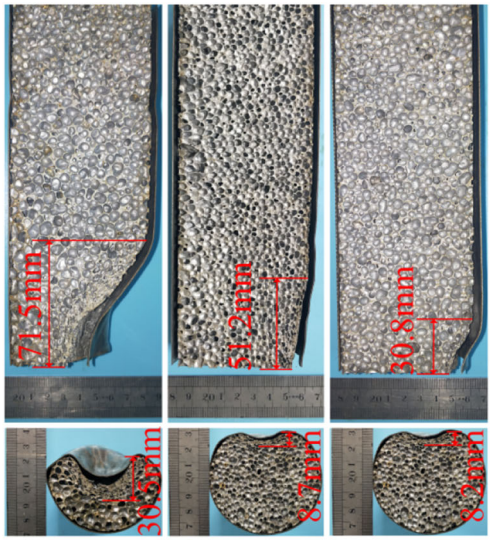

Test No.	10	8	9
W_s(g)	100	100	100
h(mm)	0.7	0.7	0.7
R(mm)	40	60	80
D(mm)	76	76	76
I_E(N·s)	21.2	-	-
w(mm)	54.6	12	11

Fig. 8. Photographs showing the typical failure of foam-filled tubes with different standoff distances

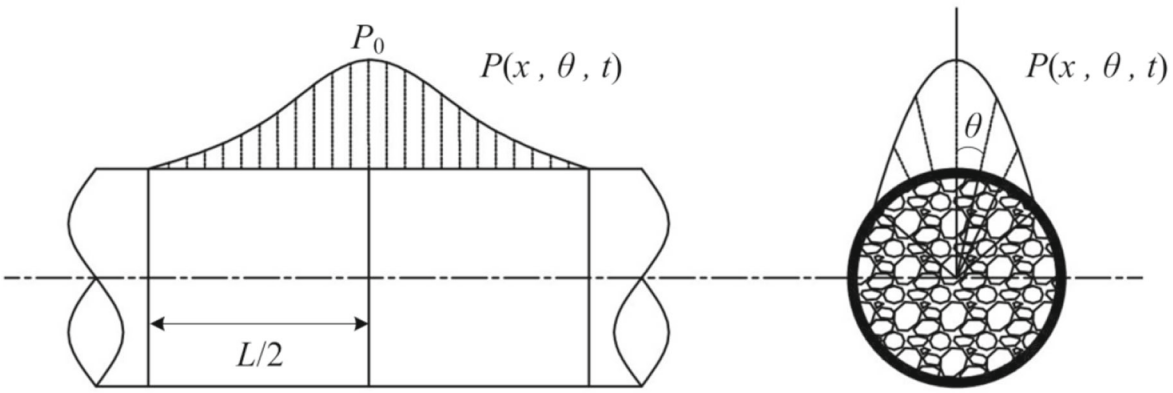

Fig. 9. Geometry and loading of the aluminum foam-filled tube

4. Numerical Simulation

4.1. FE Model

Many numerical methods have been developed for the simulation of blast loading, such as smooth particle hydrodynamics (SPH) [24], the CONWEP blast loading model [11], the arbitrary Lagrangian–Eulerian (ALE) method [25, 26], and pressure–time histories [27]. For further theoretical analysis of the structural deformation characteristics, the method of loading pressure–time history was used to simulate the deformation of the structure to keep the loading mode consistent. Also, the loading pressure–time history could control the load peak and the response time and effectively save the

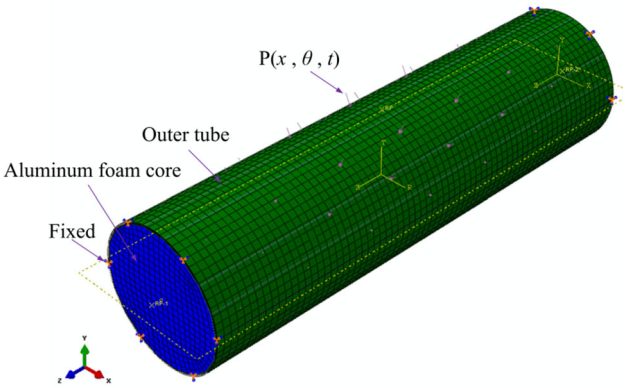

Fig. 10. Finite element model and the boundary conditions for the foam-filled tube under lateral blast loading

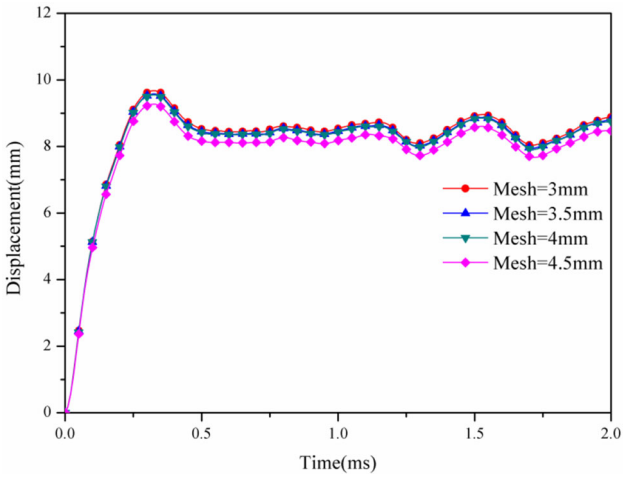

Fig. 11. The mesh convergence study results on the displacement of the outer tubes (Test No. 1)

calculation time. Therefore, Eq. (12) is employed in the upper half part of the outer tube to study the structural dynamic response under the blast impulse.

To further investigate the dynamic response and the blast resistance of foam-filled tubes, corresponding FE simulations (Fig. 10) were conducted using the ABAQUS/EXPLICIT software. The axis of the foam-filled tube was parallel to the Z-axis. A conventional 4-node shell element (S4R) was used to simulate the outer tube, and the 8-node linear solid element (C3D8R) was used to simulate the filled foam. A tie constraint was defined in the interaction between the outer tube and the foam core. At both ends of the specimen, all degrees of freedom were fixed, corresponding with the experimental loading condition. Besides, the whole calculation time was set as $t_w = 2$ ms to obtain the response process of the specimen completely.

In the FE model, the outer tube was simulated as steel with anisotropic hardening plasticity model and the density was $\rho_w = 7830\ \mathrm{kg/m^3}$, Young's modulus was $E_\mathrm{w} = 193$ GPa, Poisson's ratio was $\mu_w = 0.25$, yield stress was $\sigma_0 = 205$ MPa, and $\sigma_{UTS} = 520$ MPa at $\varepsilon_{UTS} = 0.4$. Because the relative density distribution in the aluminum foam in the production process was uneven, the average relative density of the big foam block was 15%. Therefore, the relative density of the aluminum foam was defined as 15% in the FE simulation. For the filled foam, Ruan et al. [28] produced relevant material parameters. The core was simulated as the aluminum foam with anisotropic hardening plasticity model with the density of $\rho_\mathrm{f} = 0.4\,\mathrm{g/cm^3}$, Young's modulus of $E_\mathrm{f} = 71$ MPa, and Poisson's ratio of $\mu_\mathrm{f} = 0$. Besides, a crushable foam material was defined to simulate the aluminum foam core. The plastic Poisson's ratio was $\mu_\mathrm{p} = 0.29$, and the compression yield stress ratio was $\mu_\mathrm{c} = 1.12$.

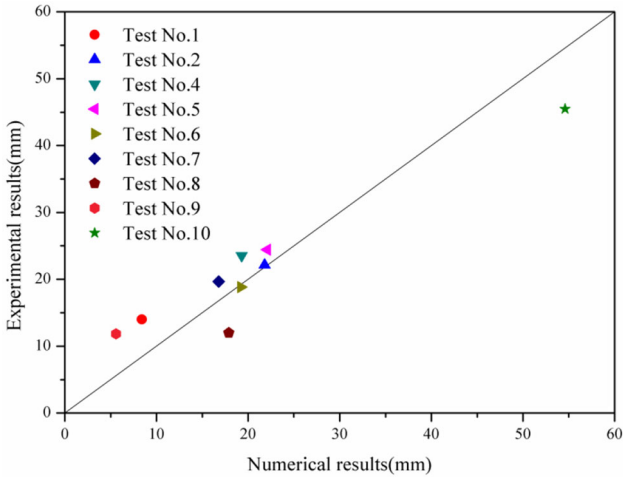

Fig. 12. Comparison between the results of the numerical simulations and the experiments for the midpoint deflection

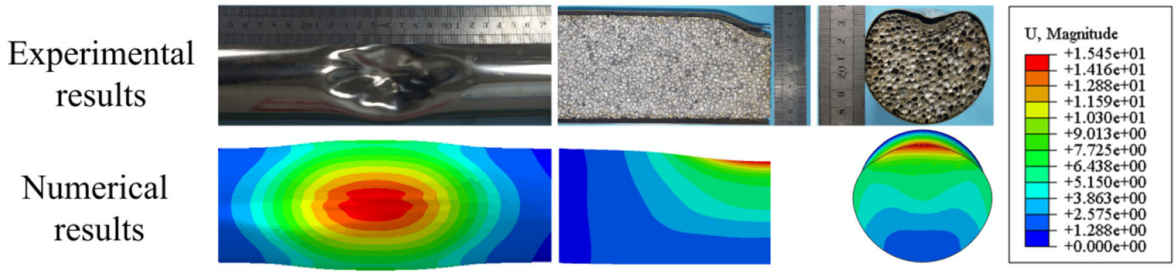

Fig. 13. Comparison between the experimental results and the numerical predictions

4.2. Verification of the FE Model

To carry out the mesh convergence study, four different element mesh sizes of 3 mm, 3.5 mm, 4 mm, and 4.5 mm were used for the foam core and the outer tube. The time-history curves of the deflection of foam-filled tubes under blast loading with four different element mesh sizes are presented in Fig. 11, showing better consistency. The mesh size of 4 mm was utilized in the numerical simulations considering computational accuracy and efficiency.

The numerical and experimental results of midpoint deflection are compared in Fig. 12. The results showed that the FE analysis results were in good agreement with the experimental results. The deflection at the midpoint in Test No. 3 shown in Fig. 12 was not obtained due to tearing of the outer tube. The difference between the simulation and experimental results might be due to the complexity of the explosion event and the limitation of the numerical method as the ideal tie constraint between the foam and the outer tube was assigned. The deformation mode of the foam-filled tubes was compared with the experimental result in Fig. 13. Due to the impact of explosive products and the effect of foam-filled crushing, there were some local impinging indentations on the surface of the tube. However, the effect of explosive products and the failure of the outer tube were not considered in the simulation, which might cause a little difference from the experimental results.

5. Discussions

In this section, the dynamic response and energy absorption characteristics of foam-filled tubes are discussed in detail by changing the diameter and wall thicknesses of the outer tube, the explosive charge mass, and the standoff distance.

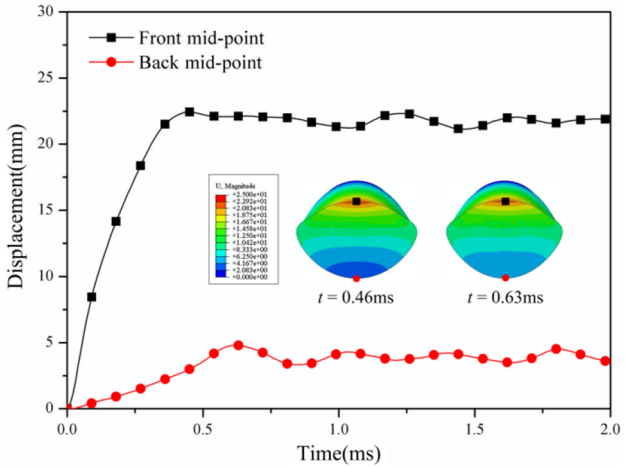

Fig. 14. Final deformation at the mid-span cross-section and corresponding time-history curves of the displacement in Test No. 2 obtained by the FE results

5.1. Deformation and Deflection

Figure 14 presents a typical dynamic response process of the foam-filled tubes in Test No. 2 ($D = 76$ mm, $h = 0.7$ mm, $W_s = 50$ g, and $R = 40$ mm). It can be seen that the maximum deflections at the front and back midpoints of the outer tube occurred at approximately 0.46 ms and 0.63 ms, respectively. After that, the deflection of the back midpoint remained constant, which marked the end of the deformation process of the entire specimen. Also, from the mid-span cross-section, it can be observed that the upper part of the model showed a larger deformation, while the deformation of the lower part was smaller. The time-history curves of the deflection at the front and back midpoints showed the same trend having small fluctuation after arriving at the peaks. The deflection at the front midpoint was significantly larger than that at the back midpoint.

Figure 15 shows the final deformation at the mid-span cross-section for different models obtained by the FE results. It can be seen that the three deformation types were observed in each model [23] including a large plastic deformation region at the central part of the structure (Type 1), a rigid section moving around the plastic hinge (Type 2), and the undistorted boundary region (Type 3). Also, the specimen had local plastic deformation under blast loading with different diameters and wall thicknesses of the outer tubes. The large plastic deformation occurred with different explosive charge masses and standoff distances. A variation in the explosive charge mass or the standoff distance had a significant influence on the deformation mode of the foam-filled tubes.

5.2. Non-dimensional Deflection

To eliminate the dimensional effect, the non-dimensional midpoint deflection on the blasting surface w_0 is defined as:

$$w_0 = \frac{w}{D} \tag{15}$$

The effects of tube diameter, wall thickness, explosive charge mass, and standoff distance on the non-dimensional midpoint deflection on the blasting surface for the foam-filled tubes were investigated as shown in Fig. 16. An increase in either the wall thickness or the diameter of the outer tube improved the stiffness of the foam-filled tubes under blast loading. As the wall thickness and diameter of the foam-filled tubes or the standoff distance decreased, the non-dimensional midpoint deflection increased. As the explosive charge mass increased, the non-dimensional midpoint deflection increased.

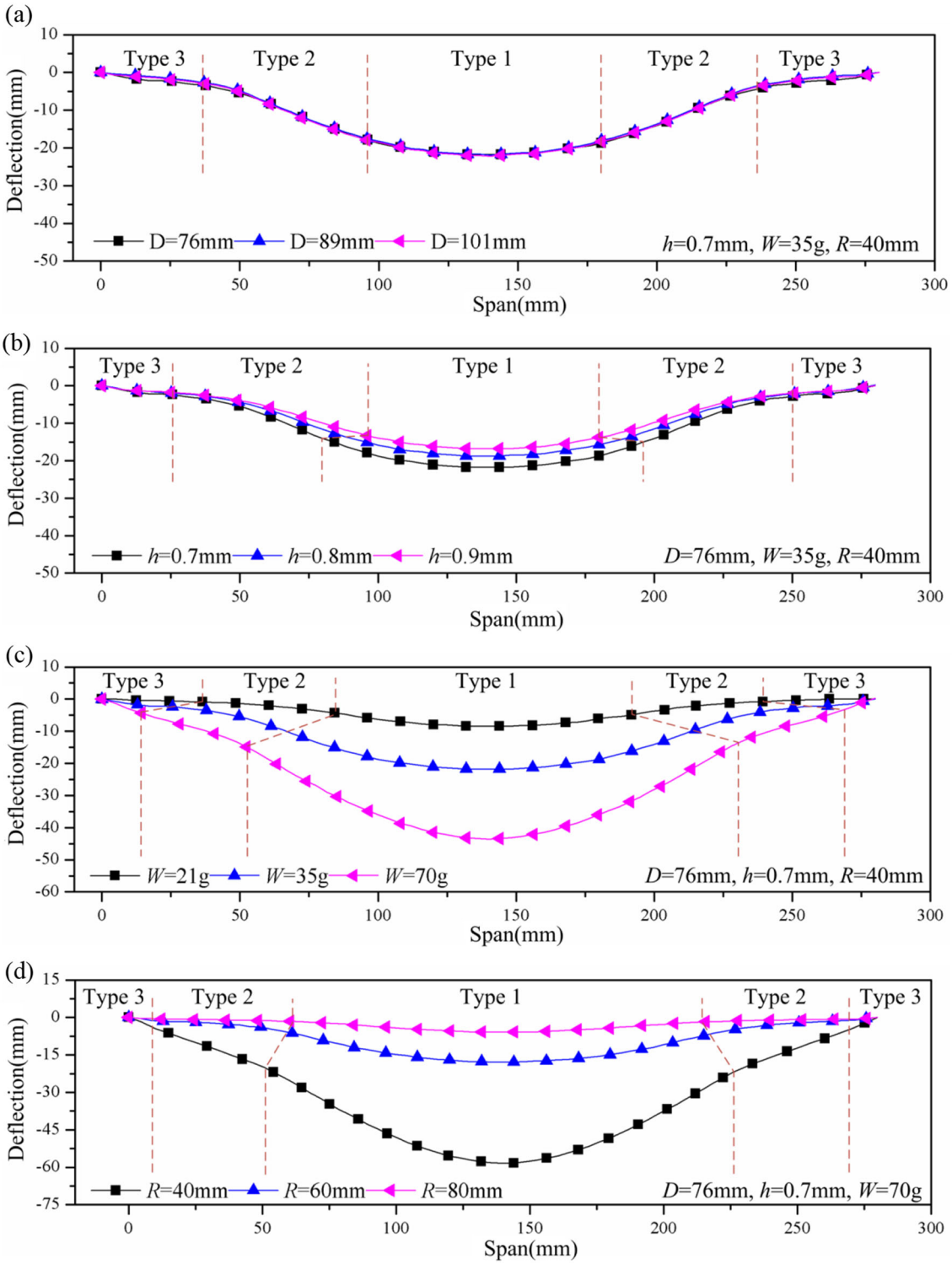

Fig. 15. Permanent deflection at the radial section of the foam-filled tubes with different **a** diameters; **b** wall thicknesses; **c** explosive charge masses; **d** standoff distances

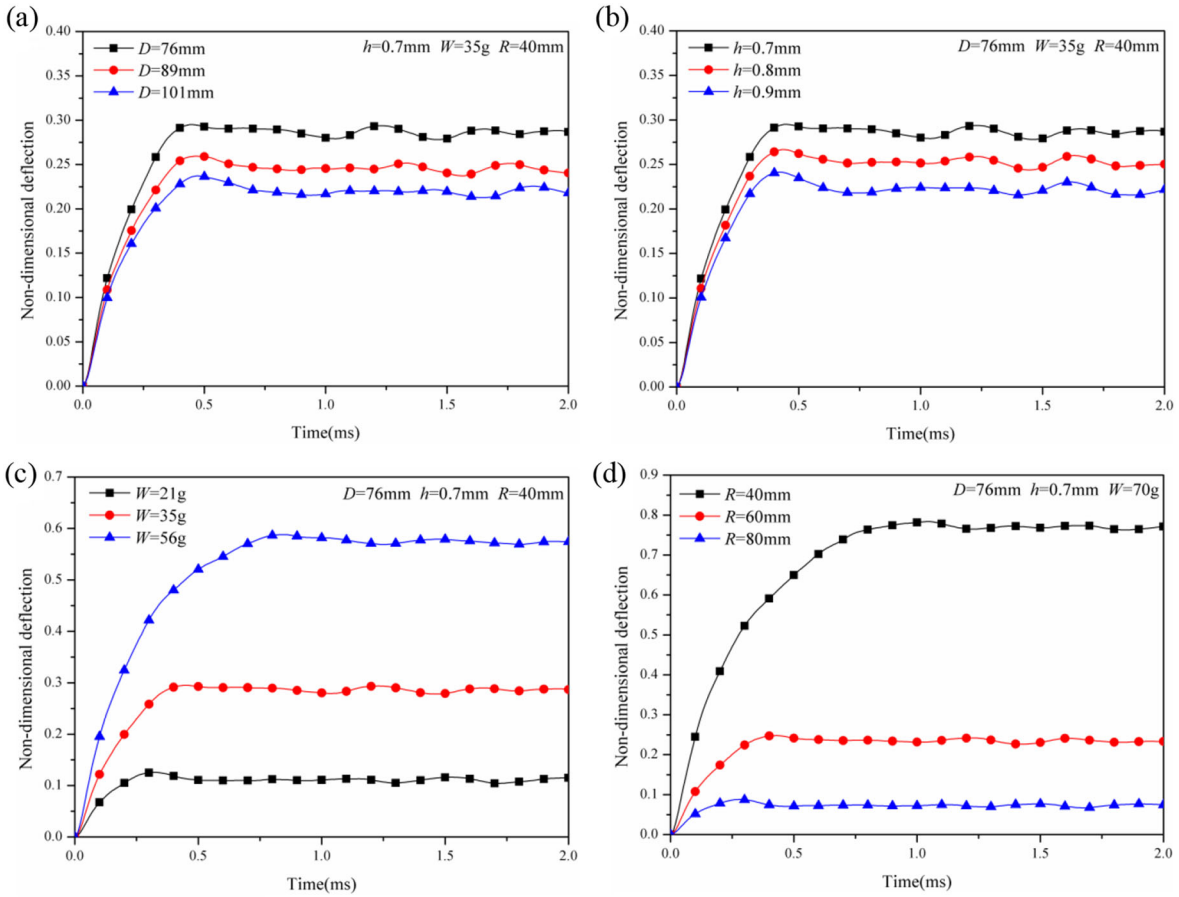

Fig. 16. The effects of **a** tube diameter; **b** wall thickness; **c** explosive charge mass; **d** standoff distance on the non-dimensional deflection of foam-filled tubes

5.3. Energy Absorption

The index of the energy absorption capacity, SEA (specific energy absorption), was used to evaluate the energy absorption of the foam-filled tubes. It is defined as follows:

$$\mathrm{SEA} = \frac{E_P}{W_0} \tag{16}$$

where E_P is the total absorbed energy, and W_0 is the mass of the test specimen. The time-history curves of deflection in Figs. 14 and 16 showed that the deflection of the whole model remained stable at $t = 2$ ms. The plastic deformation of the model was dominant when the blast loading was acted on the foam-filled tubes. Therefore, the plastic dissipation energy at $t = 2$ ms was taken as the total absorbed energy (E_P).

Figure 17 shows the comparison of the SEA values for different foam-filled tubes. It could be concluded that by fixing other parameters, the specific energy absorption of foam-filled tubes increased with an increase in the explosive charge mass. However, as the diameter and wall thickness of the outer tube or the standoff distance decreased, the energy absorption capacity of the foam-filled tubes increased.

To analyze the energy absorption of each component of the foam-filled tube in detail, the energy absorption contribution ratio n by each component to the total absorbed energy by the specimen is defined as:

$$n = \frac{E_{i,P}}{E_P} \times 100\% \tag{17}$$

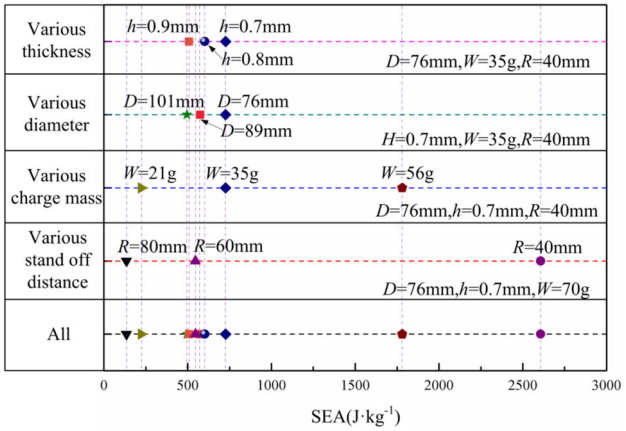

Fig. 17. Comparison of the SEA values for the foam-filled tubes with different influencing factors (the points with the same shape and color are located on the same vertical dotted line representing the same foam-filled tube)

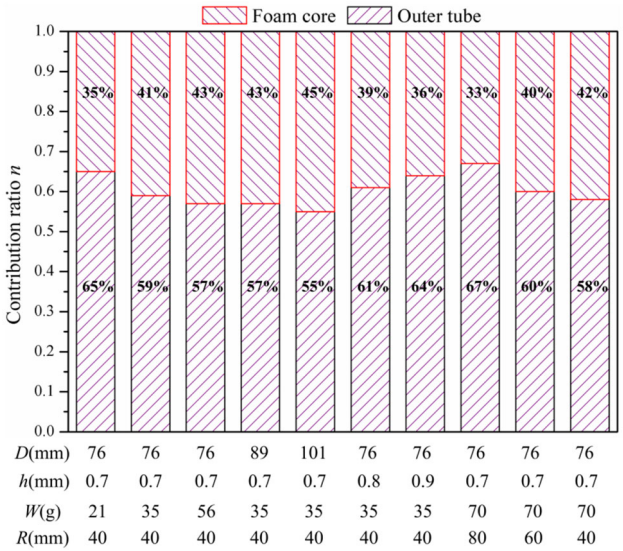

Fig. 18. The contribution ratio of the energy absorption by each component of the foam-filled tubes with different geometric parameters and explosive charge masses

where $E_{i,P}$ is the energy absorption by each component. Figure 18 shows the energy absorption contribution ratio of each component for different foam-filled tubes. It can be seen that the energy absorption by the foam core was smaller than that by the outer tube, which was the main energy absorption part. With other parameters fixed, the contribution ratio of the foam core increased with an increase in the explosive charge mass or the diameter of the outer tube. As the wall thicknesses of the outer tube or the standoff distances increased, the energy absorption capacity of the foam core decreased.

6. Conclusions

The deformation modes, blast resistance, and energy absorption of aluminum foam-filled tubes with different diameters and wall thicknesses under lateral blast loading were investigated experimentally and numerically. A four-cable ballistic pendulum system was employed to perform the blast experiment, and the FE simulations were conducted by employing the ABAQUS software. Numerical simulation results for the deformation modes and deflection of the specimens showed good agreement with the experimental results. The following conclusions could be drawn based on our results and discussions.

(1) In the blast experiment, the deformation modes of foam-filled tubes under lateral blast loading could be generally divided into local plastic deformation, large plastic deformation with an elliptical shape, and tearing of the outer tube. The deformation area of the foam-filled tubes increased with an increase in the explosive charge mass or the wall thickness, or with a decrease in the standoff distance.
(2) The introduction of the foam core had a vital effect on the energy absorption capacity of the structure. The energy absorption contribution ratio of the foam core accounted for 33–45%, which was an integral part.
(3) The numerical results showed that the explosive charge mass and the standoff distance had significant effects on the non-dimensional deflection at the midpoint of the specimen. However, the wall thickness and diameter of the outer tube had a slight influence on the non-dimensional deflection at the midpoint of the specimen. The specific energy absorption of the foam-filled tubes increased when the explosive charge mass increased or the standoff distance decreased.

Acknowledgements. This work was supported by the National Natural Science Foundation of China (11772216, 12072219 and 11902215). The financial contributions are gratefully acknowledged.

References

[1] Nia AA, Parsapour M. Comparative analysis of energy absorption capacity of simple and multi-cell thin-walled tubes with triangular, square, hexagonal and octagonal sections. Thin-Walled Struct. 2014;74:155–65.
[2] Jing L, Yang F, Zhao LM. Perforation resistance of sandwich panels with layered gradient metallic foam cores. Compos Struct. 2017;171:217–26.
[3] Song JF, Xu SC, Xu LH, et al. Experimental study on the crashworthiness of bio-inspired aluminum foam-filled tubes under axial compression loading. Thin-Walled Struct. 2020;155:106937.
[4] Hall IW, Guden M, Claar TD. Transverse and longitudinal crushing of aluminum-foam filled tubes. Trans Mater Heat Treat. 2007;46:513–8.
[5] Fan ZH, Shen JH, Lu GX, et al. Dynamic lateral crushing of empty and sandwich tubes. Int J Impact Eng. 2013;53:3–16.
[6] Shen JH, Lu GX, Ruan D, et al. Lateral plastic collapse of sandwich tubes with metal foam core. Int J Mech Sci. 2015;91:99–109.
[7] Tran T. Crushing and theoretical analysis of multi-cell thin-walled triangular tubes under lateral loading. Thin-Walled Struct. 2017;115:205–14.
[8] Wang HB, Yang JL, Liu H, et al. Internally nested circular tube system subjected to lateral impact loading. Thin-Walled Struct. 2015;91:72–81.
[9] Niknejad A, Moradi A, Beheshti N. Indentation experiments on novel sandwich composite tubes. Mater Lett. 2016;179:142–5.
[10] Liu Q, Fu J, Wang JS, et al. Axial and lateral crushing responses of aluminum honeycombs filled with EPP foam. Compos Part B: Eng. 2017;130:236–47.
[11] Li SQ, Wang ZH, Wu GY, et al. Dynamic response of sandwich spherical shell with graded metallic foam cores subjected to blast loading. Compos: Part A. 2014;56:262–71.
[12] Li SQ, Li X, Wang ZH, et al. Finite element analysis of sandwich panels with stepwise graded aluminum honeycomb cores under blast loading. Compos Part: A. 2016;80:1–12.
[13] Li SQ, Li X, Wang ZH, et al. Sandwich panels with layered graded aluminum honeycomb cores under blast loading. Compos Struct. 2017;173:242–54.
[14] Liu XR, Tian XG, Lu TJ, et al. Blast resistance of sandwich-walled hollow cylinders with graded metallic foam cores. Compos Struct. 2012;94:2485–93.
[15] Jing L, Wang ZH, Zhao LM. Dynamic response of cylindrical sandwich shells with metallic foam cores under blast loading-Numerical simulations. Compos Struct. 2013;99:213–23.
[16] Jing L, Wang ZH, Zhao LM. An approximate theoretical analysis for clamped cylindrical sandwich shells with metallic foam cores subjected to impulsive loading. Compos Part: B. 2014;60:150–7.
[17] Liang MZ, Li XY, Lin YL, et al. Multiobjective blast-resistance optimization of gradient foam sandwiched cylindrical container. Thin-Walled Struct. 2020;157:107114.
[18] Wierzbicki T, Fatt H. Damage assessment of cylinders due to impact and explosive loading. Int J Impact Eng. 1993;13:13:512-241.
[19] Song KJ, Long Y, Ji C, et al. Plastic Deformation of Metal Tubes Subjected to Lateral Blast Loads. Math Probl Eng. 2014;250379.

[20] Yuen SCK, Nurick GN, Brinckmann HB, et al. Response of cylindrical shells to lateral blast load. Int J Prot Struct. 2013;4:209–30.
[21] Jing L, Wang ZH, Shim V, et al. An experimental study of the dynamic response of cylindrical sandwich shells with metallic foam cores subjected to blast loading. Int J Impact Eng. 2014;71:60–72.
[22] Henrych J. The dynamics of explosion and its use. New York: Elsevier Scientific Publishing Company; 1979. p. 139.
[23] Li SQ, Yu BL, Karagiozova D, et al. Experimental, numerical, and theoretical studies of the response of short cylindrical stainless steel tubes under lateral air blast loading. Int J Impact Eng. 2019;124:48–60.
[24] Novak N, Starcevic L, Vesenjak M, et al. Blast response study of the sandwich composite panels with 3D chiral auxetic core. Compos Struct. 2019;210:167–78.
[25] Zhang CZ, Zhang P, Liu J, et al. Dynamic Response of Sandwich Panels With Functionally Graded Aluminum Foam Cores Subjected to Underwater Explosion. ASME International Conference on Ocean. 2016.
[26] Li X, Wang ZH, Zhu F, et al. Response of aluminium corrugated sandwich panels under air blast loadings: Experiment and numerical simulation. Int J Impact Eng. 2014;65:79–88.
[27] Karagiozova D, Nurick GN, Langdon GS. Behaviour of sandwich panels subject to intense air blasts-Part 2: Numerical simulation. Compos Struct. 2009;91:442–50.
[28] Ruan D, Lu G, Ong LS, et al. Triaxial compression of aluminium foams. Compos Sci Technol. 2007;67:1218–34.